Shear force sensing of epithelial Na^+ channel (ENaC) relies on *N*-glycosylated asparagines in the palm and knuckle domains of αENaC

Fenja Knoepp[a], Zoe Ashley[b,c], Daniel Barth[b,c], Jan-Peter Baldin[b,c], Michael Jennings[b], Marina Kazantseva[b], Eng Leng Saw[b,c], Rajesh Katare[b,c], Diego Alvarez de la Rosa[d], Norbert Weissmann[a], and Martin Fronius[b,c,1]

[a]Excellence-Cluster Cardio-Pulmonary Institute, Universities of Giessen and Marburg Lung Center, Member of the German Center for Lung Research, Justus-Liebig University Giessen, D-35392 Giessen, Germany; [b]Department of Physiology, University of Otago, 9016 Dunedin New Zealand; [c]HeartOtago, University of Otago, 9016 Dunedin, New Zealand; and [d]Department of Physiology, Institute of Biomedical Technology, University of Laguna, E-38071 La Laguna, Spain

Edited by Martin Chalfie, Columbia University, New York, NY, and approved November 26, 2019 (received for review July 2, 2019)

Mechanosensitive ion channels are crucial for normal cell function and facilitate physiological function, such as blood pressure regulation. So far little is known about the molecular mechanisms of how channels sense mechanical force. Canonical vertebrate epithelial Na^+ channel (ENaC) formed by α-, β-, and γ-subunits is a shear force (SF) sensor and a member of the ENaC/degenerin protein family. ENaC activity in epithelial cells contributes to electrolyte/fluid-homeostasis and blood pressure regulation. Furthermore, ENaC in endothelial cells mediates vascular responsiveness to regulate blood pressure. Here, we provide evidence that ENaC's ability to mediate SF responsiveness relies on the "force-from-filament" principle involving extracellular tethers and the extracellular matrix (ECM). Two glycosylated asparagines, respectively their *N*-glycans localized in the palm and knuckle domains of αENaC, were identified as potential tethers. Decreased SF-induced ENaC currents were observed following removal of the ECM/glycocalyx, replacement of these glycosylated asparagines, or removal of *N*-glycans. Endothelial-specific overexpression of αENaC in mice induced hypertension. In contrast, expression of αENaC lacking these glycosylated asparagines blunted this effect. In summary, glycosylated asparagines in the palm and knuckle domains of αENaC are important for SF sensing. In accordance with the force-from-filament principle, they may provide a connection to the ECM that facilitates vascular responsiveness contributing to blood pressure regulation.

mechanotransduction | shear force | extracellular tether | *N*-glycosylation | epithelial Na^+ channel (ENaC)

All living organisms have developed strategies that enable them to perceive their mechanical environment. This process is known as mechanotransduction and describes how mechanical forces that are acting on cells/organisms are translated into cellular signals. Among other transmembrane proteins, mechanosensitive ion channels are key molecules for this process (1, 2). Currently, two principles have been put forward to explain how force can activate mechanosensitive ion channels: 1) The "force-from-lipids" (3) identified by studying stretch-activated channels in bacteria (4), and 2) the "force-from-filaments" principle (5) that originates from studies of hair cells (6). The force-from-filaments principle (also known as the "tethered model") proposes the transmission of mechanical force through tethering of the ion channel proteins to internal (cytoskeletal filaments) or external filaments (extracellular matrix, ECM) as "sensing structures" (7–9). Deformation or deflection of the sensing structure will be transduced via tethers to the channel to change its conformation and thereby its activity.

There is emerging evidence for intracellular and extracellular tethers mediating mechanical activation of channels. For example, mechanical activation of the no mechanoreceptor potential C (NOMPC) channel of *Drosophila melanogaster* depends on ankyrin repeats within its N terminus that form an intracellular tether (10). The ankyrin repeats facilitate the connection to microtubules as identified for the transient receptor potential vanilloid type-1 (TRPV1) channel (11) that belongs to the same protein family as NOMPC. Evidence for extracellular tethers as constituents of mechanotransduction originates from studies in auditory/vestibular hair cells and *Caenorhabditis elegans* (7, 12).

In hair cells, extracellular tethers are known as tip links and were identified by electron microscopy (6, 13). Tip links are suggested to be filamentous protein structures that are directly involved in channel gating as identified in neurons that mediate touch sensation (14). Although the existence of tethers is beyond dispute, their architecture is largely unknown.

In *C. elegans*, mutations of genes encoding ion channel subunits (e.g., mechanosensory abnormality-4 [MEC-4] and MEC-10) and extracellular proteins (e.g., MEC-5 and MEC-9, which are considered to be part of the ECM) resulted in touch-insensitive animals (15, 16). This indicates that channel proteins and the ECM are connected—via tethers—to facilitate the mechanical perception of touch in *C. elegans*. The mechanosensitive MEC channel proteins of *C. elegans* are the founding members of the epithelial Na^+ channel (ENaC)/degenerin (DEG) protein family. Members of this family are widely expressed in the animal kingdom and form mechanosensitive ion channels (17). A well-known member of the family constitutes the ENaC in vertebrates (18, 19). Canonical ENaC is a heterotrimer composed of α-, β-, and γ-subunits (20)

Significance

The ability to sense mechanical forces is essential for all living organisms. Extracellular tethers have been proposed to mediate mechanical activation of channels belonging to the epithelial Na^+ channel (ENaC)/degenerin protein family. The nature and architecture of the tethers that link the channel protein with the extracellular matrix are unknown. Our study provides experimental evidence that glycosylated asparagines and their *N*-glycans are part of tethers for mechanical activation of ENaC by shear force. The identified asparagines are also important for arterial blood pressure regulation in vivo. These findings provide insights into how mechanical forces are sensed by mechanosensitive ENaC channels to regulate blood pressure.

Author contributions: F.K. and M.F. designed research; F.K., Z.A., D.B., J.-P.B., and M.J. performed research; M.K., R.K., D.A.d.l.R., and N.W. contributed new reagents/analytic tools; F.K., Z.A., D.B., J.-P.B., E.L.S., R.K., and M.F. analyzed data; and F.K. and M.F. wrote the paper.

The authors declare no competing interest.

This article is a PNAS Direct Submission.

[1]To whom correspondence may be addressed. Email: martin.fronius@otago.ac.nz.

This article contains supporting information online at https://www.pnas.org/lookup/suppl/doi:10.1073/pnas.1911243117/-/DCSupplemental.

First published December 23, 2019.

and is highly abundant in absorbing epithelia. In the kidney epithelium, ENaC is crucial for electrolyte/fluid-homeostasis (21) and blood pressure regulation (22). Soon after discovering the molecular identity of ENaC (23), evidence emerged that ENaC is mechanosensitive and activated by membrane stretch (24–27), which would be in accordance with the force-from-lipids principle. However, these studies were critically discussed (28), suggesting that there is not enough evidence to conclude that ENaC is mechanically activated by stretch.

In contrast to the controversial findings about the activation by membrane stretch, there is compelling evidence that ENaC is mechanically regulated by shear force (SF) (29–31), a frictional force caused by particles moving parallel to a surface. ENaC subunits are expressed in endothelial cells of arteries (32), arterial baroreceptors (33, 34), and distal kidney epithelium (35) where they are permanently exposed to SF due to the fluids flowing over the surface of the cells. SF has been shown to activate ENaC by increasing the channel's open probability (36, 37). Moreover, SF was identified to regulate ENaC in isolated kidney tubules (38) and arteries (39). SF sensation in both tissues is of considerable importance for blood pressure regulation (22). However, knowledge about the mechanisms of how ENaC and related ENaC/DEG channels senses SF is yet unknown.

Since ENaC proteins were identified to be related to the mechanosensitive proteins of *C. elegans*, it was hypothesized that mechanical activation involves the ECM as well as extracellular tethers that facilitate the interdependent activity (40, 41), a hypothesis that is in agreement with the force-from-filament principle. However, despite the observations from touch-insensitive *C. elegans* strains, experimental evidence for the function and architecture of extracellular tethers is scarce. Therefore, our study focuses on two aspects: 1) Providing functional evidence for the interdependent activity of the channel and the ECM for mechanical activation; and 2) identifying anchoring points for tethers within the channel, which facilitate the interaction with the ECM.

Results

In accordance with previous studies, increased activity of expressed human ENaC was identified in response to a laminar fluid flow that causes SF on the surface of cells. This was observed in *Xenopus* oocytes (Fig. 1 *A–C* and *SI Appendix*, Fig. S1*A*), HEK293 cells (*SI Appendix*, Fig. S1 *D* and *E*), and human pulmonary microvascular endothelial cells (HPMECs) (Figs. 2*G* and 3*F*). The SF-effect in oocytes was not affected by an enhanced Na^+ supply (*SI Appendix*, Fig. S1*A*), nor did an elevation of the extracellular Na^+-concentration alter ENaC currents (*SI Appendix*, Fig. S1 *B* and *C*). Therefore, an unstirred layer effect, due to different kinetics of Na^+ supply to the channel surface (42), can be excluded.

Research on MEC and DEG channels of *C. elegans* identified that their ability to respond to force relies on the ECM (15) and a connection via tethers was proposed between the ECM and the channel (16), which is in accordance with the force-from-filament concept (5).

The role of the ECM/glycocalyx for mechanical activation of ENaC is yet unknown. Therefore, we performed experiments in *Xenopus* oocytes, HEK293 cells, HPMECs, and isolated arteries from mice to address this question. The integrity of the oocyte ECM was impaired by ECM-degrading enzymes followed by the quantification of the SF effect (Fig. 2 *A* and *B*). Elastase-treatment and mechanical removal of the vitelline envelope had no effect. In contrast, hyaluronidase—which cleaves hyaluronic acid, a ubiquitous component of the ECM (43)—decreased the SF-mediated activation of ENaC. This was observed in oocytes that were treated with the enzyme before (Fig. 2 *A* and *B*) and after expression of ENaC (Fig. 2 *C–F*). Electron and fluorescence microscopy confirmed the impairment of extracellular structures at the surface of the oocytes following hyaluronidase treatment (*SI*

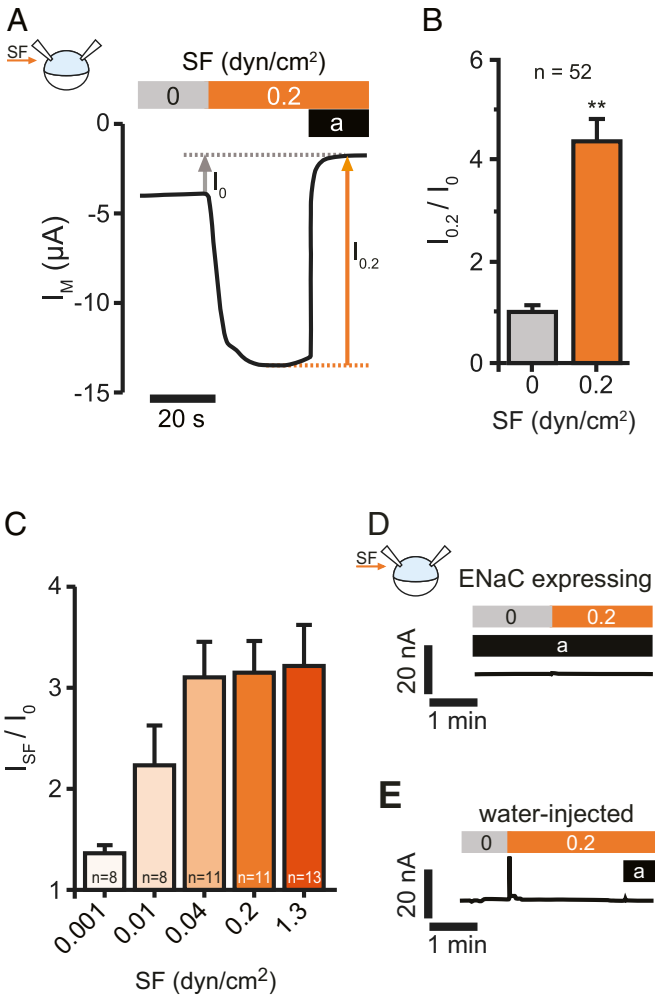

Fig. 1. ENaC is activated by SF. (*A*) Representative recording of SF application on αβγENaC currents in *Xenopus* oocytes. Activating the bath perfusion (0.2 dyn/cm^2, orange bar) induced a rapid increase of the transmembrane current (I_M). Amiloride (a, black bar) was applied to estimate ENaC-mediated current in the absence (I_0) and presence ($I_{0.2}$) of SF. (*B*) Current values with SF were normalized with respect to the values before SF was applied ($I_{0.2}/I_0$). (mean ± SEM; $^{**}P < 0.01$, one-sample *t* test, two-tailed). (*C*) The SF-response (I_{SF}) was augmented by increases in SF. (*D*) SF has no effect in the presence of amiloride (a, black bar, 10 µM), when ENaCs are blocked. (*E*) Neither SF nor amiloride affect endogenous ion channels of *Xenopus* oocytes. Oocytes were treated identical although no cRNA was dissolved in the water used for injection (representative traces of at least 12 recordings using oocytes from at least three different animals).

Appendix, Figs. S2 *A–F* and S3). Interestingly, the reduction of ENaC current with acute hyaluronidase perfusion was only observed when combined with SF. In contrast, no effect was observed when hyaluronidase was applied by manually pipetting the enzyme into the chamber (resembling under 0 dyn/cm^2) (*SI Appendix*, Fig. S2 *G–I*).

In HEK293 cells transfected with human αβγENaC, approximately two-thirds of the cells did not respond to SF, although amiloride-sensitive currents were observed (*SI Appendix*, Fig. S1 *D* and *E*). The reasons for the inconsistent effects are unknown.

For this reason, we performed whole-cell patch-clamp recordings on HPMECs. Here, similar to the observations in *Xenopus* oocytes, a robust SF-response was observed. This SF response was blunted by hyaluronidase-treatment (Fig. 2 *G* and *I*) to degrade the endothelial glycocalyx (a luminal carbohydrate-rich ECM of endothelial cells) that is known as arterial shear sensor

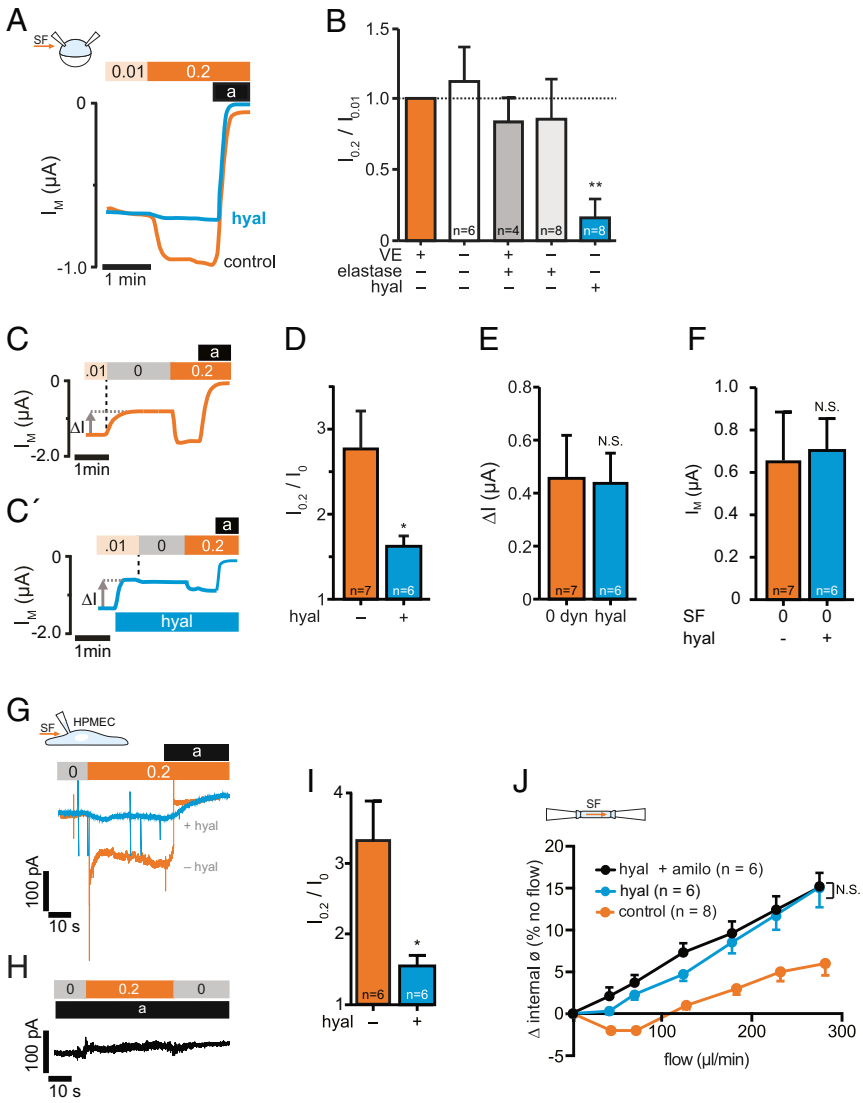

Fig. 2. SF-mediated activation of ENaC is impaired by degradation of hyaluronic acid. (*A*) Hyaluronidase treatment before expression of ENaC impaired the SF response (hyal, blue line) in comparison to untreated oocytes (control, orange line). (*B*) Averaged SF-responses ($I_{0.2}/I_{0.01}$) from oocytes following removal/degradation of ECM components (VE, vitelline envelope). SF-responses were normalized to corresponding control oocytes (intact ECM, orange bar) using cells from the same animals (mean ± SEM; $^{**}P < 0.01$, one-sample *t* test, two-tailed). (*C*) Stopping the bath perfusion (0.01 → 0 dyn/cm^2, indicated by a vertical dashed line) induced a current decrease (ΔI) and the subsequent application of SF (0 → 0.2 dyn/cm^2) resulted in a current increase. (*C′*) The application of hyaluronidase (blue bar) in the presence of SF induced a similar effect on ΔI than stopping the bath perfusion (*E*), whereas the normalized SF-effect was reduced (*D*). (*F*) Membrane currents recorded in the absence of SF (0 dyn/cm^2) were similar between oocytes that were untreated (–) or treated (+) with hyaluronidase (hyal, mean ± SEM; N.S., not significant, unpaired *t* test, two-tailed). (*G*) Current-traces of HPMECs, exposed to SF (0.2 dyn/cm^2, orange bar). Amiloride (a, black bar) was used to estimate ENaC-mediated currents. Preincubation with hyaluronidase (hyal, blue trace), blunted the SF-induced increase of ENaC currents. (*H*) No SF-response was observed in the presence of amiloride (10 µM, black bar). (*I*) Statistical analysis from experiments depicted in *G*. $^{*}P < 0.05$, unpaired *t* test, two-tailed. (*J*) Effect of intraluminal flow on isolated pressurized carotid arteries from mice at mean arterial pressure of 60 mmHg. Increased intraluminal flow affected the internal diameter of the arteries under control conditions (orange). Hyaluronidase augmented the SF-induced increase of the vessel diameter (blue) and amiloride in combination with hyaluronidase (black) had no additional effect (mean ± SEM; $^{*}P < 0.05$, N.S., not significant, repeated-measures two-way ANOVA).

(44). Furthermore, the SF response was absent in the presence of amiloride, indicating that the SF response is caused by ENaC (Fig. 2*H*). In addition, indication for successful degradation of the endothelial glycocalyx was observed by reduced fluorescence-labeled wheat germ agglutinin (WGA) staining following hyaluronidase treatment (*SI Appendix*, Fig. S3 *A*, *C*, and *D*).

Last but not least, hyaluronidase treatment of intraluminally perfused isolated carotid arteries augmented SF-induced vasodilation (Fig. 2*J*). The lack of an additional effect of amiloride when combined with hyaluronidase suggests that the activity of ENaC and the endothelial glycocalyx in response to SF is interdependent. These observations identify the role of the ECM/glycocalyx for the SF-dependent activation of ENaC in an expression system, primary endothelial cells, and arteries.

In addition to an impaired SF response, the hyaluronidase treatment decreased the affinity of the expressed channels for amiloride (*SI Appendix*, Fig. S5 *D–F*), indicating that the binding affinity of amiloride is dependent on the interaction of ENaC with the ECM and suggests that this interaction facilitates ENaC gating and function.

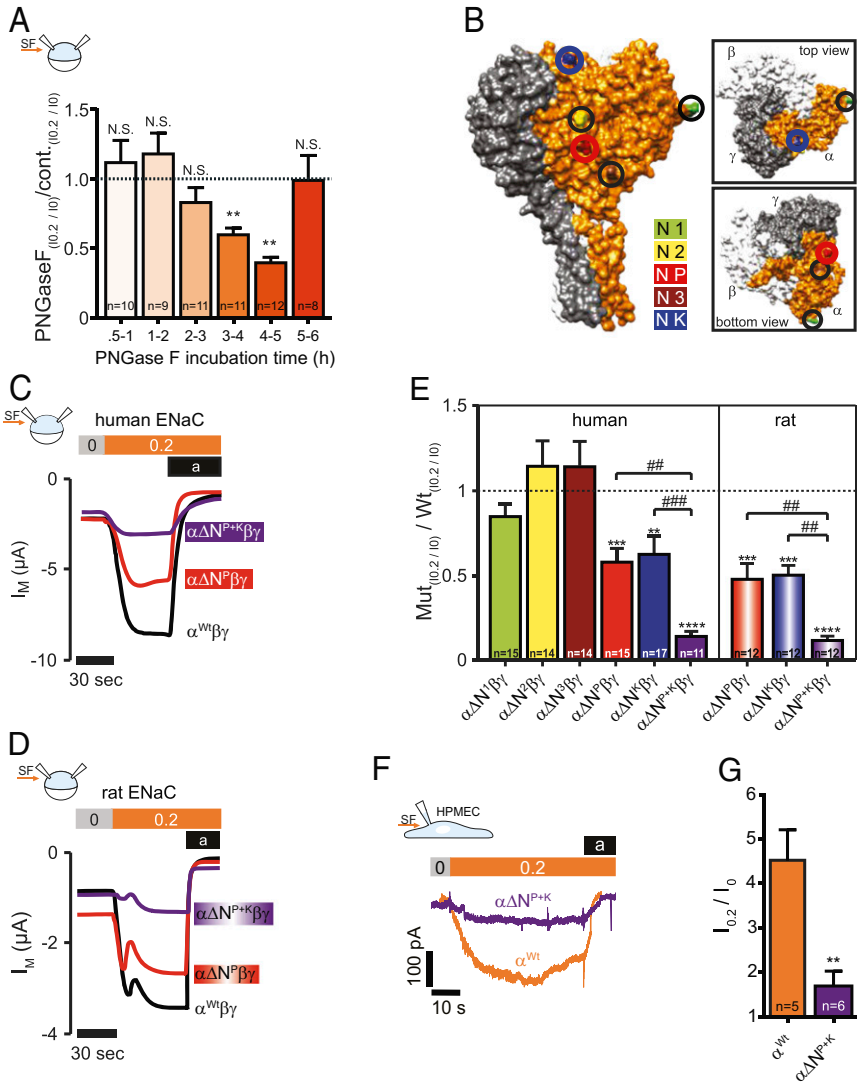

Fig. 3. *N*-linked glycans and glycosylated asparagines contribute to the SF-effect. (*A*) Injection of PNGase F into the oocytes resulted in a time-dependent reduction of the SF-mediated response (mean ± SEM; $^{**}P < 0.01$, N.S., not significant, one-sample *t* test, two-tailed). (*B*) Surface structure of a human α-, β-, γENaC-heterotrimer displaying the localization of glycosylated asparagines of αENaC. (*C*) Current-traces of the SF-effects in oocytes that express human or (*D*) αβγENaC Oocytes expressed either a wild-type (Wt) αENaC (black trace) or αENaC that had a single asparagine replaced in the palm domain ($\alpha\Delta N^{P}$, red trace) or two asparagines replaced (in palm and knuckle domain: $\alpha\Delta N^{P+K}$, purple trace). (*E*) Replacement of asparagines of human and rat αENaC in the palm and knuckle domains decreased the SF response. Dashed line represents SF responses from corresponding control experiments using either human or rat wild-type αβγENaC (mean ± SEM; $^{****}P < 0.0001$, $^{***}P < 0.001$, $^{**}P < 0.01$, one-sample *t* test, two-tailed; $^{###}P < 0.001$. $^{##}P < 0.01$ and as indicated, one-way ANOVA with Bonferroni´s multiple comparison test). (*F*) Representative current-traces of HPMECs exposed to SF (0.2 dyn/cm^2, orange bar). Amiloride (a, black bar) was applied to estimate ENaC-mediated currents. Compared to wild-type HPMECs (α^{Wt}, orange current trace), CRISPR/Cas9-mediated replacement of the asparagines in the palm and knuckle domains of αENaC ($\alpha\Delta N^{P+K}$, purple trace) blunted the SF-induced increase in current in these cells. (*G*) Statistical analysis from experiments depicted in *F*. $^{**}P < 0.01$, unpaired *t* test, two-tailed.

Extracellular *N*-Glycosylated Asparagines in the Palm and Knuckle Domains Facilitate SF Responsiveness. Although the existence of tethers for mechanotransduction of channels is well accepted, their architecture is unknown. We hypothesized that extracellular *N*-linked glycans attached to asparagines within an extracellular NXT/S motif of ENaC could be anchor points and thus part of a molecular tether contributing to SF sensation. The *N*-linked glycans may interact with other proteoglycans within the ECM and these glycan–glycan interactions can transmit SF-induced movements from the ECM to the channel. Such glycan–glycan interactions were identified to be important for the adherence of bacteria to host cells (45) and cell–cell interaction in cancer (46). In sponges, adhesive forces provided by glycan–glycan interactions are considered to maintain the multicellular integrity of the sponge (47). This supports the assumption that glycan-dependent interactions can provide the physical strength to transmit movements of the ECM/glycocalyx to the channel.

To reveal the potential role of *N*-linked glycans for SF-mediated activation of ENaC, experiments with PNGase F were performed. PNGase F targets glycosylated asparagines by cleaving the connection between the asparagine and the attached *N*-acetylglucosamine (48). ENaC-expressing oocytes were injected with PNGase F to make the enzyme intracellularly available. The ability of PNGase F to remove *N*-glycans was observed in immune blotting experiments (Fig. 4*A*). After PNGase F injection into oocytes, SF-induced currents were measured between 0.5 and 6 h after injection. Three to 5 h after the PNGase F injection, reduced SF-induced currents were observed (Fig.

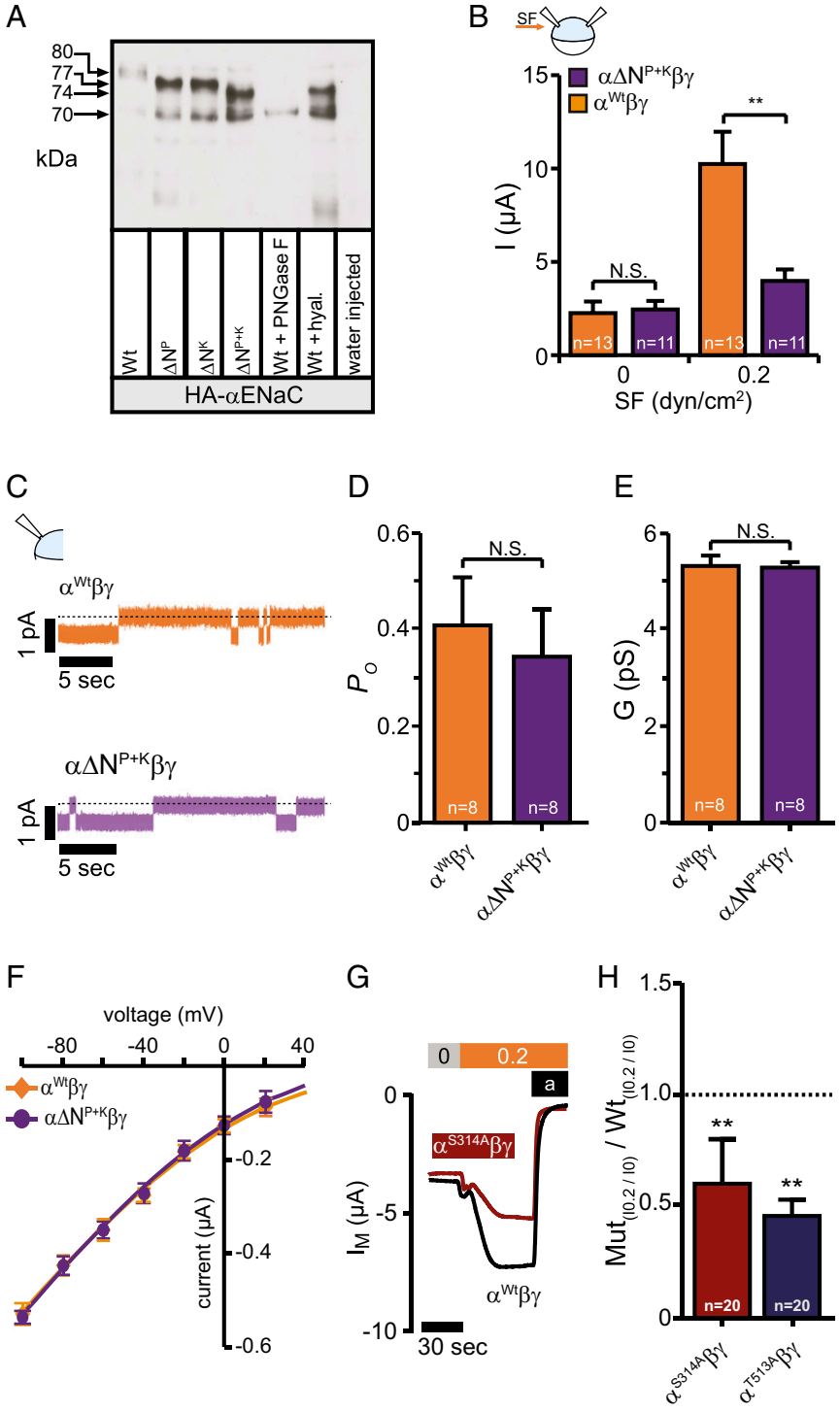

Fig. 4. *N*-linked glycans contribute to the SF-mediated effect but do not affect basic channel properties. (*A*) Immunoblotting of whole-cell lysates from oocytes expressing either HA-tagged human or wild-type αENaC (Wt) subunits with the asparagine in the palm or knuckle domains replaced or both. The shift in relative molecular mass (MR) is observed between the wild-type (~80 kDa) and the modified subunits (~77 kDa for ΔN^{P} and ΔN^{K} and ~74 kDa for ΔN^{P+K}) corresponding to a lack of *N*-linked glycosylation. Total removal of *N*-linked glycosylation by PNGase F resulted in the complete loss of the upper (glycosylated) band and shifted the band to ~70 kDa (Wt+PNGase F). Treatment of wild-type with hyaluronidase resulted in a band of ~74 kDa (Wt+hyal). Cell lysates of water-injected control-oocytes served as a control for antibody specificity. The depicted blot is representative for $n = 6$. (*B*) Amiloride sensitive currents at 0 dyn are similar, but increased in wild-type when exposed to 0.2 dyn/cm^2 SF (mean ± SEM; $^{**}P < 0.01$, N.S., not significant, 2-way ANOVA followed by Sidak's multiple comparison test). (*C*) Current-traces of cell attached single-channel recordings at a membrane-potential of -100 mV using devitellinized oocytes. (*D–F*) Neither the open probability (P_O), the conductance (*G*), nor the single-channel current voltage relationship was affected by replacement of the asparagines. Means were fitted by the Goldman–Hodgkin–Katz equation. The calculated permeability for Na^+ was wild-type: 1.72 × 10−12 cm^{-3} s^{-1}; $\alpha\Delta N^{P+K}\beta\gamma$ENaC: 1.73 × 10−12 cm^{-3} s^{-1} (mean ± SEM; N.S., not significant, unpaired *t* test, two-tailed). (*G* and *H*) Disruption of the glycosylation motif in the palm and knuckle domains did reduce the SF-mediated effect (mean ± SEM; $^{**}P < 0.01$, one-sample *t* test, two-tailed).

3*A*). The reduced currents were not caused by overall reduced ENaC currents (e.g., due to impaired channel trafficking). This is supported by similar amiloride-sensitive currents despite reduced SF responses (*SI Appendix*, Fig. S4*D*).

In another approach, *N*-glycosylated asparagines within the extracellular region of αENaC, which is crucial for forming effective channels (49), were substituted by site-directed mutagenesis. The human subunit has five conserved asparagines in its extracellular domain within an NXT/S motif (Fig. 3*B* and *SI Appendix*, Fig. S4*A*). These asparagines were replaced individually against alanines to remove *N*-linked glycans aiming to prevent their interaction with ECM/glycocalyx components. Subsequent assessment of the SF-mediated currents revealed that channels lacking an asparagine in the palm ($\alpha\Delta N^{P}$) or knuckle ($\alpha\Delta N^{K}$) domains had an ∼40% lower SF-mediated current compared with channels containing the wild-type αENaC subunit (Fig. 3 *C* and *D* and *SI Appendix*, Fig. S4*E*). In addition, increased IC_{50} values for amiloride were observed after replacement of N^{P} or N^{K} (*SI Appendix*, Fig. S5*G*). This is in agreement with the increased IC_{50} for amiloride observed after degradation of hyaluronic acid (*SI Appendix*, Fig. S5 *D–F*), indicating that a physical interaction between channel and the ECM facilitates channel function. Removal of this interaction by either degrading the ECM or removal of *N*-glycans affects the amiloride binding affinity and is indicative for altered channel gating. This is in agreement with observations that alterations within the extracellular domain, such as the DEG site of ENaC, can affect the amiloride binding affinity and gating of ENaC (50).

Replacement of both asparagines simultaneously ($\alpha\Delta N^{P+K}$) had additive effects on the SF response. This indicates that the asparagine in the palm (N^{P}) and knuckle (N^{K}) domains facilitate the SF response independent of each other (Fig. 3 *C–E*). The role of these asparagines for facilitating SF-responsiveness of ENaC is conserved between species, because similar effects were observed when replacing the corresponding asparagines of rat αENaC (Fig. 3 *D* and *E*). The combined replacement of N^{P} with the remaining three asparagines (N1, N2, N3) had no additive effect (*SI Appendix*, Fig. S4*E*). These experiments identify *N*-glycosylated asparagine in the palm and knuckle domains of αENaC to be important for SF-mediated activation of ENaC in *Xenopus* oocytes.

To further reveal the role of these asparagines for SF activation of ENaC in endothelial cells, experiments with HPMECs were performed. Here, the corresponding asparagines were replaced by a CRISPR/Cas 9 genome-editing approach and SF-induced currents were recorded and compared to control cells. Similar to the observations in oocytes we observed a significant reduced SF response in cells that expressed the $\alpha\Delta N^{P+K}$ in comparison to cells expressing the wild-type αENaC subunit (Fig. 3 *F* and *G*).

Additional experiments were performed in oocytes to reveal whether the proposed asparagines are glycosylated and if 1) their removal affects channel function beside the ability to respond to SF and 2) to reveal if the asparagines or the attached *N*-linked glycans are important for SF activation.

To reveal if the asparagines are glycosylated, immunoblotting was performed to compare the molecular mass of $\alpha\Delta N^{P}$, $\alpha\Delta N^{K}$, and $\alpha\Delta N^{P+K}$ with regard to the wild-type subunit. The wild-type αENaC subunit containing an HA-tag for detection was detected at ∼80 kDa, whereas the PNGase F-treated sample had a molecular mass of 70 kDa (Fig. 4*A*). The proteins with N^{P} or N^{K} replaced were detected at ∼77 kDa and the protein with both asparagines replaced had a band at ∼74 kDa. This indicates that the replacement of the asparagines does decrease the molecular mass, likely due to the lack of *N*-linked glycans. It may also be noted that the SF responses of the HA-tagged subunits (wild-type and mutated) were similar (*SI Appendix*, Fig. S5*A*) in comparison with the untagged proteins (Fig. 3*D*).

Evidence suggests that replacement of multiple glycosylated asparagines influence ENaC function or trafficking (51). To account for this possibility, amiloride-sensitive whole-cell currents as a measure of functional channels on the membrane, single-channel open probability, and conductance of channels containing $\alpha\Delta N^{P+K}$ were analyzed and compared to α^{Wt}-, β-, γENaC. In the absence of SF, neither whole-cell amiloride-sensitive currents (Fig. 4*B*) nor the open probability (Fig. 4 *C* and *D*) and conductance (Fig. 4 *E* and *F*) were affected by the replacement of the asparagines. These findings are further supported by surface biotinylation experiments. Here the membrane abundance of $\alpha\Delta N^{P+K}$ was similar in both *Xenopus* oocytes and HPMECs, each in comparison to the respective control cells expressing α^{Wt} (*SI Appendix*, Fig. S5 *B* and *C*). This indicates that the replacements of the two asparagines affects neither channel function in the absence of SF nor membrane abundance.

To reveal the importance of the *N*-glycans vs. asparagines, αENaC mutations were generated where the glycosylation motif for N^{P} and N^{K} was disrupted. Expression of each of these αENaC subunits with β and γ provided reduced SF-mediated currents (Fig. 4 *G* and *H*), similar to the effect observed with the replaced asparagines (Fig. 3*D*).

Overall, the outcome of these experiments using *Xenopus* oocytes and HPMECs indicates that the *N*-glycans attached to the asparagines in the palm and knuckle domains of αENaC are important for the ability of ENaC in response to SF but do not impair other channel functions.

Glycosylated Asparagines in the Palm and Knuckle Domains Contribute to Arterial Blood Pressure Regulation. Growing evidence suggests that ENaC expressed in endothelial cells is involved in blood pressure regulation, independent from its known role in the kidneys (22). The observations in primary human endothelial cells (Figs. 2*G* and 3*F*) and isolated arteries (Fig. 2*J*) imply that these *N*-glycosylated asparagines may contribute to the SF sensation ability of ENaC and the regulation of the vascular tone. To address this putative role, normal healthy mice were transduced with adenoviral vectors (AdVs). The animals were divided in three groups defined by the viral construct containing either: 1) The wild-type αENaC subunit (α^{Wt}), 2) $\alpha\Delta N^{P+K}$ ENaC (asparagines in the palm and knuckle domains replaced), or 3) an empty vector (control, no ENaC). The transgene-expression was under the control of the vascular endothelial cadherin promotor, which directs the αENaC transgene to be specifically expressed in endothelial cells. Blood pressure and heart rate were measured in conscious mice before and after the adenoviral transduction.

Blood pressures of animals of all three groups before transduction were similar (Fig. 5*A*). After overexpression, α^{Wt} caused an increased systolic blood pressure by 42 ± 6 mmHg (Fig. 5*A*). Overexpression of $\alpha\Delta N^{P+K}$ increased the blood pressure by 11 ± 2 (mmHg), which was considerably smaller compared with animals overexpressing α^{Wt}. In $\alpha\Delta N^{P+K}$ the increased blood pressure seems to reflect increased ENaC in arteries, but due to the impaired SF responsiveness, the increase in blood pressure is smaller in comparison to animals transduced with α^{Wt}. Transduction with the empty vector did not affect blood pressure (Fig. 5*A*). Neither the heart rate (Fig. 5*B*) nor the body or organ weight (*SI Appendix*, Fig. S6 *A* and *B*) was affected in either group by the transduction. The increase in blood pressure in animals overexpressing α^{Wt} was already associated with impaired vascular (Fig. 5*E*) and cardiac function (Fig. 5*F*). Pressure myography on carotid arteries revealed decreased flow-mediated dilation in α^{Wt} animals in comparison to $\alpha\Delta N^{P+K}$ and control (Fig. 5*E*). In addition, a reduced ejection fraction of the heart was observed (Fig. 5*F*), corresponding with an increased residual blood volume in the left ventricle due to decreased fractional shortening (*SI Appendix*, Fig. S6 *E* and *F*). These effects were not seen in $\alpha\Delta N^{P+K}$ and control animals. The changes in cardiac function in α^{Wt} were not associated with structural

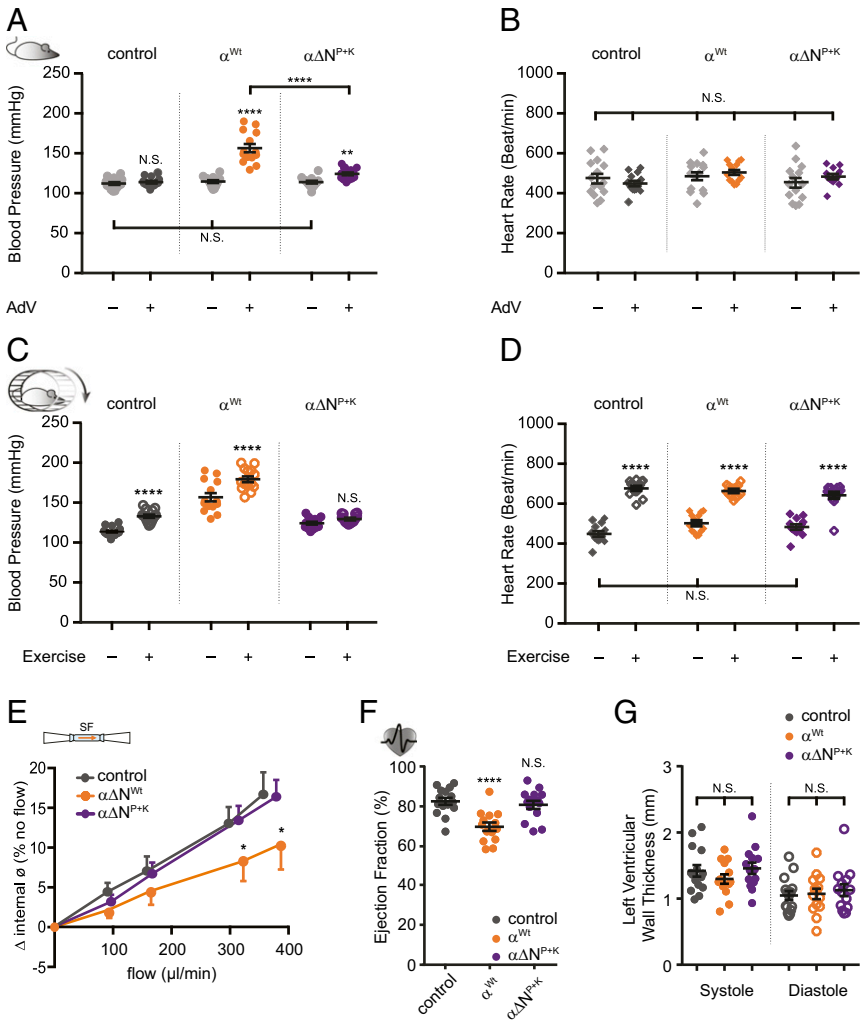

Fig. 5. Blood pressure increase after viral transduction relies on glycosylated asparagines. (*A*) Systolic blood pressure from three groups recorded before and after viral transduction. The increase in blood pressure was smaller in animals that received an αENaC subunit lacking asparagines in the palm and knuckle domains ($\alpha\Delta N^{P+K}$, purple; mean ± SEM; ****$P < 0.0001$, **$P < 0.01$, N.S., not significant, 2-way ANOVA followed by Tukey's multiple comparison test). (*B*) The heart rate of the animals was not affected by the viral transduction. (*C*) Replacement of asparagines prevented the increase in blood pressure in response to exercise. (*D*) Changes in heart rate during exercise were not affected (mean ± SEM; ****$P < 0.0001$, **$P < 0.01$, N.S., not significant, two-way ANOVA followed by Tukey´s multiple comparison test). (*E*) Flow-mediated vasodilation was blunted in carotid arteries isolated from animals that received the wild-type αENaC subunit ($n = 5$; orange), whereas those of $\alpha\Delta N^{P+K}$ were protected ($n = 7$; purple; control: $n = 5$; dark gray; mean ± SEM; *$P < 0.05$, two-way ANOVA with Newman Keul's multiple comparison test). (*F*) The increased blood pressure by αENaC transduction was accompanied by changes of the heart function including reduced ejection fraction (mean ± SEM; N.S., not significant, ****$P < 0.0001$, one-way ANOVA with Tukey's multiple comparison test). (*G*) Changes of the heart structure (ventricular wall thickness) were not observed (mean ± SEM; N.S., not significant, one-way ANOVA with Tukey's multiple comparison test).

changes of the heart (*SI Appendix*, Fig. S6 *G* and *H*), as indicated by unchanged left ventricular wall thickness (Fig. 5*G*).

To further determine the potential effect of increased SF on blood pressure, animals were subjected to exercise on a treadmill in order to increase their heart rate and blood pressure. The transduction of α^{Wt} and control vector was associated with a further increase in blood pressure in response to treadmill exercise (Fig. 5*C*). Interestingly, in mice overexpressing $\alpha\Delta N^{P+K}$ this exercise-induced increase in blood pressure was not observed (Fig. 5*C*). However, all three groups responded to exercise by a similar increase of the heart rate (Fig. 5*D*). In summary, these experiments in mice indicate that N^P and N^K contribute to blood pressure regulation in vivo.

Discussion

In this study, we demonstrated that mechanical activation of ENaC in response to SF depends on an intact ECM/glycocalyx and extracellular *N*-glycosylated asparagines. Impairment of the integrity of either the ECM or glycocalyx, replacement of asparagines in the palm and knuckle domains of the αENaC subunit, and the removal of *N*-glycans impaired the response to SF. This indicates an interdependent activity between the ECM/glycocalyx and ENaC. This is in agreement with the force-from-filament principle (5), where the ECM represents the extracellular sensing structure, the channel containing asparagines as anchor points are the "receiver," and the *N*-glycans attached to asparagines represent the filament/tether. Evidence for this architectural feature of mechanotransduction was observed studying human, mouse, and rat ENaC function in vitro. It is further supported by evidence that it is important for the regulation of blood pressure in vivo.

N-glycosylated asparagines are a common posttranslational modification (52), primarily known to influence channel maturation and trafficking (53), including ENaC (51). Furthermore,

N-glycans attached to asparagines are considered to add new functional features to proteins without changing the amino acid sequence (52). Besides protein maturation and trafficking, *N*-glycans are described as adhesion molecules. They facilitate cell–cell interactions, either via glycan–glycan or glycan–protein interactions (54). Protein *N*-glycans are associated with maintaining tissue integrity (47) to support the assumption that *N*-linked glycosylated asparagines and their *N*-glycans are suitable tethers for mechanotransduction. We could also speculate that changes of the *N*-glycans represent an ability to modulate interaction with the ECM and therefore mechanotransduction. This is indicated by observations that cancer cells have altered *N*-glycans and this is associated with impaired contact inhibition and cancer progression (46). We could speculate that this aspect also accounts for the variability of the SF response in immortalized cells such as HEK293 cells.

We propose a role for *N*-glycosylated asparagines as anchoring points for tethers for mechanotransduction that is in accordance with the force-from-filament principle. This mechanism is not only limited to the sensation of SF caused by the flow of liquids over cell surfaces. The *N*-glycan based connection with the ECM/glycocalyx can also facilitate the sensation of touch and cellular responses to pressure. Deflection of the ECM/glycocalyx in response to touch and changes in pressure can cause a relative movement of the ECM/glycocalyx with respect to the cell membrane to produce lateral movement that is similar to the effect of SF causing lateral deflection.

This role of *N*-glycosylated asparagines may also contribute to mechanical activation of ion channels such as acid-sensing ion channels or ATP-gated P2X4 channels that share a similar structure with ENaC (55–57) and are suggested to form mechanosensitive channels (12, 58–60). Furthermore, mechanosensitivity of ion channels, such as PIEZO1 (61) and TRP channels, may also rely on *N*-glycosylated asparagines. PIEZO1 is a shear sensor in the vasculature (62) and is activated by membrane stretch in accordance to the force from lipid principle (63). The study by Cox et al. (63) also reveals that the stretch activation of PIEZO1 can be modulated by the cytoskeleton, which is in agreement with the force-from-filament principle although the connection to the cytoskeleton does reduce PIEZO1's mechanosensitivity. Interestingly, PIEZO1 has three peripheral domains known as "blades" that are crucial for mechanical activation (64). Interestingly, the extracellular loops 15 and 16 within the blade are important for mechanical activation. Their removal did not affect membrane localization, only the mechanical activation was impaired. This is in agreement with our observations that replacement of ΔN^{P} and ΔN^{K} of αENaC affects the SF response but does not interfere with membrane localization. Although important for mechanical activation, loops 15 and 16 of PIEZO1 do not seem to interact with the lipid bilayer. This opens up the possibility that these loops may facilitate/modulate mechanical activation of PIEZO1 via an interaction with the ECM. This possibility is supported by a study providing evidence that ECM components are important for mechanical activation of PIEZO1 (65), indicating that the channel interacts with the ECM and thus may also be influenced by extracellular filaments. It may be hypothesized that extracellular *N*-glycosylated asparagines may contribute to this interaction.

However, removal of the *N*-glycosylated asparagines does not completely diminish the SF response. This indicates that the role of the identified asparagines is not an all or none response and also suggests that other mechanisms contribute to SF activation of ENaC, including the force-from-lipid principle, given that initial reports showed evidence for stretch-induced activation (24). Nevertheless the identified *N*-glycosylated asparagines are important modulators for SF responsiveness. In addition, the function of *N*-glycosylated asparagines for mechanotransduction may depend on their specific localization within a protein, because only two of the five asparagines did change the SF response. This indicates a specific role for some asparagines and their attached *N*-glycans, respectively, rather than a general role of *N*-glycan/ECM interaction.

The Physiological Role of Interdependent ENaC/ECM Activity. The results obtained in our study are of considerable relevance for various physiological processes and, as demonstrated, blood pressure regulation in particular. The endothelial glycocalyx is crucial for mechanotransduction of SF in blood vessels (66, 67). Here SF regulates the local production and release of the vasodilator nitric oxide (68). This enables local autonomous modulation of the vascular tone by adjusting the vessel diameter to alterations in blood perfusion rates (68). Strikingly, ENaC in endothelial cells exerts its effects by influencing nitric oxide production (69, 70). Thus, SF may cause deflections of the endothelial glycocalyx that in turn is transmitted via *N*-glycans to αENaC, where it changes the open probability of the channel that affects nitric oxide production (via yet unknown mechanisms) and thus the vascular tone of arteries. Evidence from this study provides insights that extends the role of *N*-glycosylated asparagines of proteins. This role as anchor points for molecular tethers is highly relevant for mechanotransduction processing of channels but may also facilitate molecular interactions that are a prerequisite for normal cell function.

Materials and Methods

Detailed information on the experimental methods can be found in *SI Appendix*.

Experimental Animals and Ethical Approval. All experiments were approved by the University of Otago's Animal Ethics Committee and conducted in accordance with the New Zealand Animal Welfare Act (approval nos. 114/13, 83/16, ET17/14, and 34/17).

Heterologous Expression of ENaC in *Xenopus* Oocytes. ENaCs were heterologously expressed in *Xenopus laevis* oocytes, as previously described (36, 71). Briefly, cRNA encoding the human or rat α-, β-, γENaC-subunits were injected at a ratio of 1:1:1 (0.9 ng for human or 2.1 ng for rat ENaC/oocyte) und used for two-electrode voltage-clamp (TEVC) recordings within 24 to 48 h.

TEVC. TEVC recordings were performed as described previously (36). SF was applied in physiologically relevant ranges (0.001 to 1.3 dyn/cm^2) by increasing the perfusion velocity in a customized perfusion chamber.

Site-Directed Mutagenesis. Point mutations were introduced in plasmid constructs containing the coding sequence for human or rat αENaC subunit using a commercial site-directed mutagenesis kit. Mutagenesis was confirmed by sequencing (Eurofins). cRNA was generated by in vitro transcription.

CRISPR/Cas9-Mediated Gene Editing in HPMECs. Trueguide one-piece modified single-guide RNA was complexed with Platinum Cas9 Protein and codelivered to HPMECs with single-stranded CRISPR-HDR templates by lipofectamine CRISPRMAX. Putative off-target effects were examined via CasOffFinder and cleavage efficiency in HPMECs validated via GeneArt Genomic Cleavage Detection Kit. Mutations were introduced sequentially. HPMECs were either used for patch-clamp electrophysiology or surface biotinylation followed by immunoblotting. Point mutations were verified by sequencing.

Molecular Structure and Localization of Glycosylated Asparagines within the Human ENaC. The selected asparagines within the cryoelectron microscopy structure of ENaC [PDB ID code 6BQN (20)] were visualized by using University of California, San Francisco Chimera 1.10.2 (http://www.cgl.ucsf.edu/chimera; Resource for Biocomputing, Visualization, and Informatics, University of California, San Francisco, supported by National Institute of General Medical Sciences P41-GM103311) (72). To indicate the accessibility of the selected asparagines, the "surface" function was utilized to visualize the solvent-accessible surface area (Connolly surface).

Determination of ENaC Glycosylation by Western Blot. Protein extracts were obtained from oocytes expressing C-terminal HA-tagged αENaC. For deglycosylation, protein extracts were treated with hyaluronidase or PNGase F,

denaturated, and separated by SDS/PAGE. Proteins were then transferred onto nitrocellulose-membranes and detected with antibodies directed against its C-terminal HA-tag. Bands were visualized using a customized enhanced chemiluminescence solution and captured on photoreactive films.

Biotinylation of αENaC Subunits on the Cell Surface. All biotinylation steps were performed on ice in a 4 °C cold room using 75 *Xenopus* oocytes per group. After 15-min incubation in biotinylation buffer, oocytes were washed with Quench buffer, MBS, and lysed. The whole-cell protein was transferred to 50 μL PierceTM Neutravidin UltraLink and rotated overnight. Samples were boiled for 10 min at 95 °C loaded on SDS/PAGE gel (Bio-Rad, TGX FastCast Acrylamide Solutions). Following transfer to PVDF-membranes, bands were visualized and their intensities quantified.

Removal of ECM Components of *Xenopus* Oocytes. The extracellular matrix of *Xenopus* oocytes consists of 1) the vitelline envelope and 2) filamentous, glycocalyx-like structures within the perivitelline space (73). The vitelline envelope was removed as previously described (36, 74). ECM-components within the perivitelline space were targeted enzymatically by incubation in either hyaluronidase or elastase. PNGase F was dissolved in an intracellular-like solution and injected into the oocytes and the SF responses of these oocytes were compared with matched water-injected time controls.

Transmission Electron Microscopy of *Xenopus* Oocytes. Oocytes were fixed with 2% glutaraldehyde in sodium cacodylate buffer with the addition of 1,600 ppm ruthenium hexamine trichloride. Samples were washed and postfixed with 1% Osmium tetroxide, including 1,600 ppm ruthenium hexamine trichloride, followed by en bloc staining with 1% uranyl acetate and dehydration through a graded progressive series of acetone concentrations, and embedded overnight in EMBed812 resin before polymerization, then erially sectioned at 100 nm using a Reichart Ultracut E microtome; ribbons were collected and viewed on a Philips CM100.

WGA Staining of the Cellular Glycocalyx. *Xenopus* oocytes and HPMECs were incubated in hyaluronidase-containing solution, fixed with formaldehyde and stained with WGA-OregonGreen488-conjugate. The ECM/glycocalyx-thickness and WGA-fluorescence intensity was visualized by confocal microscopy and analyzed with ImageJ.

Patch-Clamp Experiments.

Single-channel recordings. Single-channel recordings were performed in the cell-attached configuration on devitellinized ENaC-expressing oocytes in a high K^+ bath to depolarize the membrane potential and a high Na^+ pipette solution. Single-channel currents were recorded at −100 mV, amplified, acquired, and analyzed as previously described (36).

Whole-cell recordings on HPME cells. HPMECs were grown in medium supplemented with 100 nM Dexamethasone for 72 h prior to experiments. Experiments were performed at room temperature and SF (0.2 dyn/cm^2) was applied via a pipette tip connected to a gravity-driven perfusion system. Amiloride was applied to estimate ENaC-mediated currents and whole-cell currents recorded at −60 mV.

Whole-cell recordings on HEK293 cells. HEK293 were treated with the DNA mix (plasmids encoding the human α-, β-, and γENaC subunit and enhanced green fluorescent protein). Experiments were performed within 18 to 32 h after transfection. Whole-cell currents were recorded at −60 mV at room temperature.

Gene Transfer via AdVs in Mice. Gene transfer to endothelial cells was performed by an intravenous injection of commercial AdVs to overexpress the murine αENaC (either α^{Wt}, $\alpha\Delta N^{P+K}$, or an empty vector) driven by vascular endothelial cadherin promoter. Mice (C57BL/6, 18 male and 27 female, 11- to 13-wk-old) were randomized into three groups (15 mice each). Each mouse received a single tail-vein injection of 5×10^{11} vector genomes dissolved in 250 μL PBS.

Measurement of Blood Pressure by Tail Cuff. The systolic blood pressure and heart rate were recorded via tail cuff prior to AdV transduction and 1 wk after AdV injection. Blood pressure was measured at rest and after exercise.

Echocardiography. Cardiac function was assessed by echocardiography in mice under anesthesia using a VIVID E9 cardiovascular ultrasound system fitted with an 11-MHz probe. Left ventricular wall thickness, left ventricular volume (end-systolic, end-diastolic, and stroke volume), systolic function (internal diameter, ejection fraction, fractional shortening, and cardiac output) were assessed as previously described (75). At least three independent 2D-targeted M-mode measurements were obtained for each animal from the short-axis view.

Pressure Myography. Pressure myography was performed as previously described (39). Briefly, carotid arteries were mounted in the pressure myograph system and internal and external vessel diameter was captured at 60-mmHg intraluminal pressure. Flow and resulting SF rates were applied by a pressure gradient between the inlet and outlet pressure transducer and were determined by a flow meter (DMT 162FM) integrated into the system. Amiloride was used to determine ENaC mediated vascular responses and hyaluronidase to degrade the endothelial glycocalyx.

Statistical Analysis. Data are presented as mean ± SEM. Numbers of individual experiments are declared as *n*. The number of animals from which oocytes were used was ≥2. Statistical analysis was performed with Prism GraphPad. $P \leq 0.05$ was considered as statistically significant.

Data Availability Statement. All data discussed in this paper will be made available to readers by the corresponding author on reasonable request.

ACKNOWLEDGMENTS. The authors thank Allan Mitchell and Sharon Lequeux for assistance with the electron microscopy; Siegfried Kristek, Leo van Rens, and James Woods for excellent mechanical support; Dr. Ines Fonfara, Dr. Simone Kaut, Dr. Monika Brosien, Dr. Christine Veith-Berger, and Dr. Joe Yip for providing constructive advice; Alexander Perniss and Dr. Oleg Pak for their valuable support regarding confocal microscopy; Susanne Lich, Carmen Homberger, Nils Schupp, Karin Quanz, and Ingrid Breitenborn-Müller for technical assistance; Dr. Mike Althaus and Dr. Pawel Piotr Szczesniak for providing early structures for protein models and comments for editing early drafts of the manuscript; and Dr. Fiona McDonald, Dr. Kirk L. Hamilton, and Dr. Boris Martinac for their valuable comments and suggestions during editing and finalizing of the manuscript. This work was supported by the Department of Physiology, University of Otago (AIM Fund), a University of Otago Research Grant, government funding administered by the Royal Society of New Zealand (Marsden Fund; 15-UOO-030), and a Lottery Health Research Grant (2016-25773 to M.F.). In addition D.B., J.-P.B., and E.L.S. were supported by a University of Otago PhD Scholarship, and F.K. was supported by a Post-Graduate Scholarship from the University Giessen.

1. O. P. Hamill, B. Martinac, Molecular basis of mechanotransduction in living cells. *Physiol. Rev.* **81**, 685–740 (2001).
2. D. E. Jaalouk, J. Lammerding, Mechanotransduction gone awry. *Nat. Rev. Mol. Cell Biol.* **10**, 63–73 (2009).
3. J. Teng, S. Loukin, A. Anishkin, C. Kung, The force-from-lipid (FFL) principle of mechanosensitivity, at large and in elements. *Pflugers Arch.* **467**, 27–37 (2015).
4. B. Martinac, J. Adler, C. Kung, Mechanosensitive ion channels of E. coli activated by amphipaths. *Nature* **348**, 261–263 (1990).
5. S. Katta, M. Krieg, M. B. Goodman, Feeling force: Physical and physiological principles enabling sensory mechanotransduction. *Annu. Rev. Cell Dev. Biol.* **31**, 347–371 (2015).
6. J. O. Pickles, S. D. Comis, M. P. Osborne, Cross-links between stereocilia in the Guinea pig organ of Corti, and their possible relation to sensory transduction. *Hear. Res.* **15**, 103–112 (1984).
7. P. G. Gillespie, R. G. Walker, Molecular basis of mechanosensory transduction. *Nature* **413**, 194–202 (2001).
8. D. Zanini, M. C. Göpfert, Mechanosensation: Tethered ion channels. *Curr. Biol.* **23**, R349–R351 (2013).
9. M. Krieg, A. R. Dunn, M. B. Goodman, Mechanical systems biology of C. elegans touch sensation. *Bioessays* **37**, 335–344 (2015).
10. W. Zhang *et al.*, Ankyrin repeats convey force to gate the NOMPC mechanotransduction channel. *Cell* **162**, 1391–1403 (2015).
11. M. Prager-Khoutorsky, A. Khoutorsky, C. W. Bourque, Unique interweaved microtubule scaffold mediates osmosensory transduction via physical interaction with TRPV1. *Neuron* **83**, 866–878 (2014).
12. M. Chalfie, Neurosensory mechanotransduction. *Nat. Rev. Mol. Cell Biol.* **10**, 44–52 (2009).
13. D. N. Furness, C. M. Hackney, Cross-links between stereocilia in the guinea pig cochlea. *Hear. Res.* **18**, 177–188 (1985).
14. J. Hu, L. Y. Chiang, M. Koch, G. R. Lewin, Evidence for a protein tether involved in somatic touch. *EMBO J.* **29**, 855–867 (2010).
15. H. Du, G. Gu, C. M. William, M. Chalfie, Extracellular proteins needed for C. elegans mechanosensation. *Neuron* **16**, 183–194 (1996).
16. L. Emtage, G. Gu, E. Hartwieg, M. Chalfie, Extracellular proteins organize the mechanosensory channel complex in C. elegans touch receptor neurons. *Neuron* **44**, 795–807 (2004).
17. I. Hanukoglu, A. Hanukoglu, Epithelial sodium channel (ENaC) family: Phylogeny, structure-function, tissue distribution, and associated inherited diseases. *Gene* **579**, 95–132 (2016).
18. C. M. Canessa, J. D. Horisberger, B. C. Rossier, Epithelial sodium channel related to proteins involved in neurodegeneration. *Nature* **361**, 467–470 (1993).

PHYSIOLOGY

19. M. Chalfie, M. Driscoll, M. Huang, Degenerin similarities. *Nature* **361**, 504 (1993).
20. S. Noreng, A. Bharadwaj, R. Posert, C. Yoshioka, I. Baconguis, Structure of the human epithelial sodium channel by cryo-electron microscopy. *eLife* **7**, e39340 (2018).
21. B. C. Rossier, M. E. Baker, R. A. Studer, Epithelial sodium transport and its control by aldosterone: The story of our internal environment revisited. *Physiol. Rev.* **95**, 297–340 (2015).
22. D. G. Warnock *et al*., Blood pressure and amiloride-sensitive sodium channels in vascular and renal cells. *Nat. Rev. Nephrol.* **10**, 146–157 (2014).
23. C. M. Canessa *et al*., Amiloride-sensitive epithelial Na+ channel is made of three homologous subunits. *Nature* **367**, 463–467 (1994).
24. M. S. Awayda, I. I. Ismailov, B. K. Berdiev, D. J. Benos, A cloned renal epithelial Na+ channel protein displays stretch activation in planar lipid bilayers. *Am. J. Physiol.* **268**, C1450–C1459 (1995).
25. J. M. Achard, J. K. Bubien, D. J. Benos, D. G. Warnock, Stretch modulates amiloride sensitivity and cation selectivity of sodium channels in human B lymphocytes. *Am. J. Physiol.* **270**, C224–C234 (1996).
26. I. I. Ismailov, B. K. Berdiev, V. G. Shlyonsky, D. J. Benos, Mechanosensitivity of an epithelial Na+ channel in planar lipid bilayers: Release from Ca2+ block. *Biophys. J.* **72**, 1182–1192 (1997).
27. H. L. Ji, C. M. Fuller, D. J. Benos, Osmotic pressure regulates alpha beta gamma-rENaC expressed in Xenopus oocytes. *Am. J. Physiol.* **275**, C1182–C1190 (1998).
28. B. C. Rossier, Mechanosensitivity of the epithelial sodium channel (ENaC): Controversy or pseudocontroversy? *J. Gen. Physiol.* **112**, 95–96 (1998).
29. L. M. Satlin, S. Sheng, C. B. Woda, T. R. Kleyman, Epithelial Na(+) channels are regulated by flow. *Am. J. Physiol. Renal. Physiol.* **280**, F1010–F1018 (2001).
30. M. D. Carattino, S. Sheng, T. R. Kleyman, Epithelial Na+ channels are activated by laminar shear stress. *J. Biol. Chem.* **279**, 4120–4126 (2004).
31. M. D. Carattino, S. Sheng, T. R. Kleyman, Mutations in the pore region modify epithelial sodium channel gating by shear stress. *J. Biol. Chem.* **280**, 4393–4401 (2005).
32. N. Golestaneh *et al*., Mineralocorticoid receptor-mediated signaling regulates the ion gated sodium channel in vascular endothelial cells and requires an intact cytoskeleton. *Biochem. Biophys. Res. Commun.* **280**, 1300–1306 (2001).
33. H. A. Drummond, M. P. Price, M. J. Welsh, F. M. Abboud, A molecular component of the arterial baroreceptor mechanotransducer. *Neuron* **21**, 1435–1441 (1998).
34. H. A. Drummond, M. J. Welsh, F. M. Abboud, ENaC subunits are molecular components of the arterial baroreceptor complex. *Ann. N. Y. Acad. Sci.* **940**, 42–47 (2001).
35. J. Loffing, V. Summa, M. Zecevic, F. Verrey, Mediators of aldosterone action in the renal tubule. *Curr. Opin. Nephrol. Hypertens.* **10**, 667–675 (2001).
36. M. Althaus, R. Bogdan, W. G. Clauss, M. Fronius, Mechano-sensitivity of epithelial sodium channels (ENaCs): Laminar shear stress increases ion channel open probability. *FASEB J.* **21**, 2389–2399 (2007).
37. S. Wang, F. Meng, S. Mohan, B. Champaneri, Y. Gu, Functional ENaC channels expressed in endothelial cells: A new candidate for mediating shear force. *Microcirculation* **16**, 276–287 (2009).
38. T. Morimoto *et al*., Mechanism underlying flow stimulation of sodium absorption in the mammalian collecting duct. *Am. J. Physiol. Renal. Physiol.* **291**, F663–F669 (2006).
39. Z. Ashley, S. Mugloo, F. J. McDonald, M. Fronius, Epithelial Na^+ channel differentially contributes to shear stress-mediated vascular responsiveness in carotid and mesenteric arteries from mice. *Am. J. Physiol. Heart Circ. Physiol.* **314**, H1022–H1032 (2018).
40. M. Fronius, W. G. Clauss, Mechano-sensitivity of ENaC: May the (shear) force be with you. *Pflugers Arch.* **455**, 775–785 (2008).
41. H. A. Drummond, N. L. Jernigan, S. C. Grifoni, Sensing tension: Epithelial sodium channel/acid-sensing ion channel proteins in cardiovascular homeostasis. *Hypertension* **51**, 1265–1271 (2008).
42. D. Mackay, P. Meares, On the correction for unstirred solution films in ion-exchange membrane cells. *Kolloid Z.* **167**, 31–39 (1959).
43. J. D. Humphrey, E. R. Dufresne, M. A. Schwartz, Mechanotransduction and extracellular matrix homeostasis. *Nat. Rev. Mol. Cell Biol.* **15**, 802–812 (2014).
44. M. Y. Pahakis, J. R. Kosky, R. O. Dull, J. M. Tarbell, The role of endothelial glycocalyx components in mechanotransduction of fluid shear stress. *Biochem. Biophys. Res. Commun.* **355**, 228–233 (2007).
45. C. J. Day *et al*., Glycan:glycan interactions: High affinity biomolecular interactions that can mediate binding of pathogenic bacteria to host cells. *Proc. Natl. Acad. Sci. U.S.A.* **112**, E7266–E7275 (2015).
46. S. S. Pinho, C. A. Reis, Glycosylation in cancer: Mechanisms and clinical implications. *Nat. Rev. Cancer* **15**, 540–555 (2015).
47. O. Popescu, I. Checiu, P. Gherghel, Z. Simon, G. N. Misevic, Quantitative and qualitative approach of glycan-glycan interactions in marine sponges. *Biochimie* **85**, 181–188 (2003).
48. G. E. Norris, T. J. Stillman, B. F. Anderson, E. N. Baker, The three-dimensional structure of PNGase F, a glycosylasparaginase from Flavobacterium meningosepticum. *Structure* **2**, 1049–1059 (1994).
49. C. M. Canessa, A. M. Merillat, B. C. Rossier, Membrane topology of the epithelial sodium channel in intact cells. *Am. J. Physiol.* **267**, C1682–C1690 (1994).
50. S. Kellenberger, I. Gautschi, L. Schild, An external site controls closing of the epithelial Na+ channel ENaC. *J. Physiol.* **543**, 413–424 (2002).
51. O. B. Kashlan *et al*., N-linked glycans are required on epithelial Na^+ channel subunits for maturation and surface expression. *Am. J. Physiol. Renal. Physiol.* **314**, F483–F492 (2018).
52. A. Helenius, M. Aebi, Intracellular functions of N-linked glycans. *Science* **291**, 2364–2369 (2001).
53. D. Baycin-Hizal *et al*., Physiologic and pathophysiologic consequences of altered sialylation and glycosylation on ion channel function. *Biochem. Biophys. Res. Commun.* **453**, 243–253 (2014).
54. A. Varki, Glycan-based interactions involving vertebrate sialic-acid-recognizing proteins. *Nature* **446**, 1023–1029 (2007).
55. J. Jasti, H. Furukawa, E. B. Gonzales, E. Gouaux, Structure of acid-sensing ion channel 1 at 1.9 A resolution and low pH. *Nature* **449**, 316–323 (2007).
56. E. B. Gonzales, T. Kawate, E. Gouaux, Pore architecture and ion sites in acid-sensing ion channels and P2X receptors. *Nature* **460**, 599–604 (2009).
57. T. Kawate, J. C. Michel, W. T. Birdsong, E. Gouaux, Crystal structure of the ATP-gated P2X(4) ion channel in the closed state. *Nature* **460**, 592–598 (2009).
58. K. Yamamoto *et al*., Impaired flow-dependent control of vascular tone and remodeling in P2X4-deficient mice. *Nat. Med.* **12**, 133–137 (2006).
59. S. Kessler, W. G. Clauss, M. Fronius, Laminar shear stress modulates the activity of heterologously expressed P2X(4) receptors. *Biochim. Biophys. Acta* **1808**, 2488–2495 (2011).
60. D. Barth, M. Fronius, Shear force modulates the activity of acid-sensing ion channels at low pH or in the presence of non-proton ligands. *Sci. Rep.* **9**, 6781 (2019).
61. J. Ge *et al*., Architecture of the mammalian mechanosensitive Piezo1 channel. *Nature* **527**, 64–69 (2015).
62. J. Li *et al*., Piezo1 integration of vascular architecture with physiological force. *Nature* **515**, 279–282 (2014).
63. C. D. Cox *et al*., Removal of the mechanoprotective influence of the cytoskeleton reveals PIEZO1 is gated by bilayer tension. *Nat. Commun.* **7**, 10366 (2016).
64. Q. Zhao *et al*., Structure and mechanogating mechanism of the Piezo1 channel. *Nature* **554**, 487–492 (2018).
65. B. M. Gaub, D. J. Müller, Mechanical stimulation of Piezo1 receptors depends on extracellular matrix proteins and directionality of force. *Nano Lett.* **17**, 2064–2072 (2017).
66. P. F. Davies, Hemodynamic shear stress and the endothelium in cardiovascular pathophysiology. *Nat. Clin. Pract. Cardiovasc. Med.* **6**, 16–26 (2009).
67. C. Hahn, M. A. Schwartz, Mechanotransduction in vascular physiology and atherogenesis. *Nat. Rev. Mol. Cell Biol.* **10**, 53–62 (2009).
68. P. F. Davies, Flow-mediated endothelial mechanotransduction. *Physiol. Rev.* **75**, 519–560 (1995).
69. F. R. Pérez *et al*., Endothelial epithelial sodium channel inhibition activates endothelial nitric oxide synthase via phosphoinositide 3-kinase/Akt in small-diameter mesenteric arteries. *Hypertension* **53**, 1000–1007 (2009).
70. J. Fels, H. Oberleithner, K. Kusche-Vihrog, Ménage à trois: Aldosterone, sodium and nitric oxide in vascular endothelium. *Biochim. Biophys. Acta* **1802**, 1193–1202 (2010).
71. M. Fronius, R. Bogdan, M. Althaus, R. E. Morty, W. G. Clauss, Epithelial Na+ channels derived from human lung are activated by shear force. *Respir. Physiol. Neurobiol.* **170**, 113–119 (2010).
72. E. F. Pettersen *et al*., UCSF Chimera—A visualization system for exploratory research and analysis. *J. Comput. Chem.* **25**, 1605–1612 (2004).
73. C. A. Larabell, D. E. Chandler, The extracellular matrix of Xenopus laevis eggs: A quick-freeze, deep-etch analysis of its modification at fertilization. *J. Cell Biol.* **107**, 731–741 (1988).
74. C. Vitzthum, W. G. Clauss, M. Fronius, Mechanosensitive activation of CFTR by increased cell volume and hydrostatic pressure but not shear stress. *Biochim. Biophys. Acta* **1848**, 2942–2951 (2015).
75. R. Katare *et al*., Intravenous gene therapy with PIM-1 via a cardiotropic viral vector halts the progression of diabetic cardiomyopathy through promotion of prosurvival signaling. *Circ. Res.* **108**, 1238–1251 (2011).